

A Simplified Model for Buckling and Post-Buckling Analysis of Cu Nanobeam Under Compression

Jiachen Guo^{1,2}, Yunfei Xu², Zhenyu Jiang^{1,*}, Xiaoyi Liu² and Yang Cai^{2,*}

¹Department of Engineering Mechanics, South China University of Technology, Guangzhou, 510640, China

²The Peac Institute of Multiscale Sciences, Chengdu, 610031, China

*Corresponding Authors: Zhenyu Jiang. Email: zhenyujiang@scut.edu.cn; Yang Cai. Email: caiy@pims.ac.cn

Received: 22 April 2020; Accepted: 11 August 2020

Abstract: Both of Buckling and post-buckling are fundamental problems of geometric nonlinearity in solid mechanics. With the rapid development of nanotechnology in recent years, buckling behaviors in nanobeams receive more attention due to its applications in sensors, actuators, transistors, probes, and resonators in nanoelectromechanical systems (NEMS) and biotechnology. In this work, buckling and post-buckling of copper nanobeam under uniaxial compression are investigated with theoretical analysis and atomistic simulations. Different cross sections are explored for the consideration of surface effects. To avoid complicated high order buckling modes, a stress-based simplified model is proposed to analyze the critical strain for buckling, maximum deflection, and nominal failure strain for post-buckling. Surface effects should be considered regarding critical buckling strain and the maximum post-buckling deflection. The critical strain increases with increasing nanobeam cross section, while the maximum deflection increases with increasing loading strain but stays nearly the same for different cross sections, and the underlying mechanisms are revealed by our model. The maximum deflection is also influenced by surface effects. The nominal failure strains are captured by our simulations, and they are in good agreement with the simplified model. Our results can be used for helping design strain gauge sensors and nanodevices with self-detecting ability.

Keywords: Nanobeam; buckling; post-buckling; simplified model; atomistic simulation

1 Introduction

Buckling is a fundamental problem of geometric nonlinearity in solid mechanics [1]. Although in most cases buckling occurs in an elastic state, deformation (i.e., the post-buckling deformation) is more difficult to predict than that under general loading (e.g., tension, bending and torsion) [2]. With the rapid development of nanotechnology in recent years, nanobeams have been widely used as sensors, actuators, transistors, probes, and resonators in nanoelectromechanical systems (NEMS) and biotechnology [3]. Nanodevices less than 10 nm [4] have been fabricated and applied. Therefore, buckling of nanobeams is almost inevitable in practical applications [5],



This work is licensed under a Creative Commons Attribution 4.0 International License, which permits unrestricted use, distribution, and reproduction in any medium, provided the original work is properly cited.

and understanding post-buckling becomes more and more important [6]. In addition, since the dimensions of nanobeam are at the nanoscale, there exists considerable material nonlinearity induced by surface effects [7]. Understanding buckling of nanobeams is not only a fundamental problem in solid mechanics for understanding the deformation of solids with both geometric and material nonlinearities [8–10], but also of great significance to applications [11]. Early studies focused on the stability of nanobeam (e.g., the critical strain and stress) [12–14]. The surface effects on the elastic properties of nanobeam are considered as surface stresses based on surface constitutive equations [15]. This method has been successfully used to resolve some problems related to vibration, bending and buckling stability of nanobeam [16]. However, post-buckling deformation of nanobeam is still unclear, and of great study interest in recent years [17–20]. Compared with stability, post-buckling deformation of nanobeam is much more difficult to be predicted [21]. Post-buckling deformation of nanobeam can be affected by various factors such as surface effects, crystalline orientation and geometrical imperfection, etc. [22–24]. In most cases, these factors are coupled and thus add substantial complexities to the problem [25].

The Timoshenko beam model including surface stress effect has been widely used to analyze the post-buckling of nanobeam [21]. Surface effect is considered as nonlocal shear stress items in the governing equations [16,26]. However, for slender nanobeams, the conventional Euler buckling model is also valid [27]. Moreover, there may exist multiple buckling modes under an identical loading, which is also one issue in post-buckling analysis [28]. Although the patterns of high order buckling modes of nanobeam are more complicated than that of the first order buckling mode, the nature of their deformation is identical [29]. Therefore, understanding the first order buckling is of great importance [30]. Although buckling stability analysis of nanobeam under uniaxial compression has been relatively mature, further understanding on its post-buckling is still needed. For instance, if the deflection of nanobeam under uniaxial compression can be well described by a mechanical model, it can be potentially used as a strain gauge sensor at the nanoscale, which is important for the self-detecting ability of nanodevices in NEMS [31]. For example, according to the maximum deflection of nanobeams in a NEMS, the compression strain can be estimated. In addition, there does not exist spacing for external sensors to detect the deformation of nanobeams in a NEMS, and thus the post-buckling deformation of nanobeams can be used to characterize its work state.

In this work, the buckling and post-buckling of copper nanobeams under uniaxial compression is studied via theoretical analysis and atomistic simulations. A stress-based simplified model is proposed to analyze the critical strain for buckling, maximum deflection and nominal failure strain. This model avoids solving complicated higher-order shape functions, and directly uses a single cosine shape function. Different cross sections are explored and their similarities and differences are analyzed. For a certain length, the critical unstable strain increases with increasing cross-section dimension. In addition, we find that the surface effect plays an important role in the critical strain and post-buckling deformation of nanobeam.

2 Models and Simulation Details

Buckling is a common deformation mode which occurs when compressive stress is applied to a beam with high length-width ratio. Fig. 1 shows the loading geometry for the analysis based on classical mechanics. A pair of forces F are applied to the beam along the length direction (the x -axis). Here we focus on nanobeams with square cross sections given their wide applications in NEMS [12]. When F exceeds a critical value F_{cr} , a nanobeam is no longer stable and buckling can occur (Fig. 1b) with the introduction of perturbation (to mimic thermal fluctuations or

other local heterogeneities) in the transverse direction (the y -axis). This critical force, F_{cr} , can be obtained via classical mechanics as [1,2].

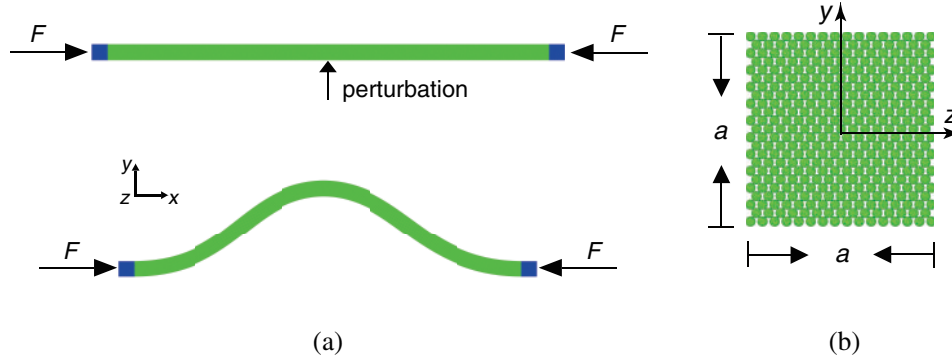


Figure 1: Schematics of Cu nanobeam for mechanical modeling and atomistic simulations. (a) Initial and post-buckling configurations, and (b) initial cross-sectional configuration. Displacement of the blue regions is fixed at zero in the y -direction and a perturbation is applied to mimic thermal fluctuations or other local heterogeneities in atomistic simulations

$$F_{cr} = \frac{4\pi^2 EI}{L_0^2}, \quad (1)$$

where E is Young's modulus, L_0 is the initial length and I is the inertia moment of the beam

$$I = \frac{a^4}{12}. \quad (2)$$

Here a is the cross-section side length. A beam is usually in elastic stage before F reaches F_{cr} , thus stress and strain normally obey a linear relation before buckling occurs. At the spatial scales of nanometer, the atomic stress is quite different from that of macroscopic scales. The non-periodic boundary conditions induce uneven distribution of the atomic stress, resulting in a larger error when using this stress to define the critical behavior. Essentially, our mechanical model is stress-based (Eq. (1)). However, we find that the solution of buckling stress is implicit. In order to facilitate the following discussion, we use buckling strain here. This method is widely used in the field of nanomechanics [32]. In this work, there is no essential difference between using buckling strain and buckling stress, since using the buckling strain is only for simplicity. Therefore, we use critical strain in following discussion. Combining Eqs. (1) and (2), we obtain the critical strain ϵ_{cr} :

$$\epsilon_{cr} = \frac{\pi^2 a^2}{3L_0^2}. \quad (3)$$

At the nanometer scale, surface effects often become prominent and should be taken into consideration. Wang and Feng's seminal model to consider the effects of residual surface tension

and shape of cross section is given as:

$$\epsilon'_{\text{cr}} = \epsilon \left(1 + \frac{8E^s}{Ea} + \frac{8^3 l^2 \tau^0}{\pi^3 a^2 Ea} \right), \quad (4)$$

where τ^0 is the residual surface tension. For both simplicity and stringency, here we consider the effects of residual surface tension and the shape of cross section [27] into an effective surface Young's modulus \tilde{E}^s , and thus an approximate form with substitution of Eq. (3) leads to

$$\epsilon'_{\text{cr}} = \frac{\pi^2 a^2}{3L_0^2} \left(1 + \frac{8\tilde{E}^s}{Ea} \right). \quad (5)$$

Unlike buckling, post-buckling is more complex and difficult to solve analytically. Here we define the nominal strain ϵ as

$$\epsilon = \frac{\delta}{L_0}, \quad (6)$$

where δ is the absolute displacement of the beam ends in the x -direction (Fig. 2). Although the patterns of high order buckling modes is more complicated than that of the first order buckling mode, the nature of their deformation is identical [29]. To investigate the underlying mechanisms of post-buckling, we focus on the most stable mode, i.e., the first order mode. A single cosine form is assumed to describe the post-buckling deformation of nanobeams to avoid complicated or high order solutions. We focus on the maximum deflection, which plays a dominant role in the deformation of nanobeams. Therefore, assuming deflection $w(L, x)$ is in a single cosine form, we obtain

$$w(L, x) = A(L) \left[1 - \cos\left(\frac{2\pi x}{L}\right) \right]. \quad (7)$$

Here $A(L)$ is the amplitude at current length in the x -direction, L . The coordinate system and relevant parameters are defined in Fig. 2. $w(L, x)$ peaks at $x = L/2$, i.e.,

$$w_{\text{max}}(L) = w\left(L, \frac{L}{2}\right) = 2A(L). \quad (8)$$

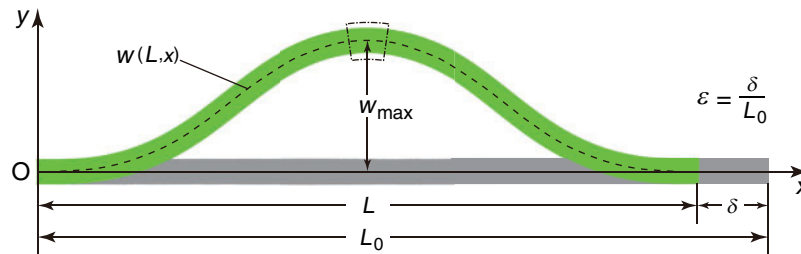


Figure 2: Definitions of the coordinate system and mechanical parameters. w : Deflection; δ : Absolute displacement of beam end in the x -direction; L_0 : Initial beam length; L : Current beam length in the x -direction. The origin is set at the center of the left end. The dashed curve denotes the central axis of the beam and the dash-dotted region corresponds to the infinitesimal element in Fig. 3

When buckling occurs, the input energy during compression loading translates into compressive or tensile strain energy in different segments of the beam along the y -axis. Under the assumption of small and isotropic deformation, the compression and tension parts are evenly split along the y -axis, and the central axis length stays unchanged. Thus, we obtain the following equation,

$$L_0 = \int_0^L \left[\left(\frac{\partial w(L, x)}{\partial x} \right)^2 + 1 \right]^{\frac{1}{2}} dx. \tag{9}$$

To satisfy the geometry relation in the above equation, $A(L)$ should increase with decreasing L . Eqs. (7) and (9) allow us to predict the shape of a beam numerically and w_{\max} is also obtained via Eq. (8) at a certain ε .

However, besides elastic energy U_e , some of the work done by external force F is converted into surface energy U_s :

$$U = U_e + U_s. \tag{10}$$

The elastic energy of nanobeam is given as:

$$U_e = \int_0^L \frac{Da}{2} \left(\frac{d^2w}{dx^2} \right)^2 dx, \tag{11}$$

where $D = Ea^3/12(1 - \nu^2)$ is bending rigidity, and ν is Poisson's ratio. The surface energy can be approximately expressed as [33]:

$$U_s = 2aL \int_0^L \left| k \frac{d^3w}{dx^3} \right| dx, \tag{12}$$

where k is a constant for surface energy increment per bending angle [34]. If the surface effects are ignored, the external work is completely converted into elastic energy, and the upper limit of w_{\max} can be obtained with Eq. (8). With the surface effect considered, the maximum deflection of nanobeam is approximately expressed as a linear decrement of maximum deflection

$$w'_{\max} \approx 2(A - \Delta A_s), \tag{13}$$

where ΔA_s is the decreased deflection due to the surface effects, and can be obtained from Eqs. (7–12):

$$\Delta A_s = 8k \sqrt{\frac{12L(1 - \nu^2)}{EU}}, \tag{14}$$

With the expressions for U_e and U_s [33], a series of implicit solutions of ΔA_s can be obtained, which demonstrates that ΔA_s is close to a constant.

The tensile and compressive stresses increase with increasing ε , and finally reach the elastic limit. We define the nominal strain when plastic failure initiates as the nominal failure strain ε_f . In order to predict ε_f for different situations, we develop a simplified model based on classical mechanics.

The local deformation at certain L and x is related to the local radius of curvature, R , defined as

$$R = \frac{dl}{d\alpha}, \quad (15)$$

where l is the arc length and α is the rotation of its tangent. For our model,

$$R(L, x) = \frac{\left[\left(\frac{\partial w(L, x)}{\partial x} \right)^2 + 1 \right]^{\frac{1}{2}} dx}{\left| d \left[\arctan \frac{\partial w(L, x)}{\partial x} \right] \right|}. \quad (16)$$

At a fixed beam geometry, R is inversely related to local deformation. Thus failure first emerges at the place with the smallest R . According to Eqs. (7) and (16), the smallest R at a certain L , $R_{\min}(L)$, is

$$R_{\min}(L) = R\left(L, \frac{L}{2}\right) = \frac{L^2}{4\pi^2 A(L)}. \quad (17)$$

Consider an infinitesimal element intercepted from Fig. 2 and illustrated in Fig. 3. The maximum compression and tension occur at the inner and outer arcs, respectively. Since most materials can bear more compression than tension, we assume failure first initiates at the outer arc. As described in Fig. 3, the outer arc length dl_{out} and central arc length dl_0 can be obtained, respectively, as

$$dl_{out}(L, a) = \left[R_{\min}(L) + \frac{a}{2} \right] d\theta, \quad (18)$$

and

$$dl_0(L) = R_{\min}(L) d\theta. \quad (19)$$

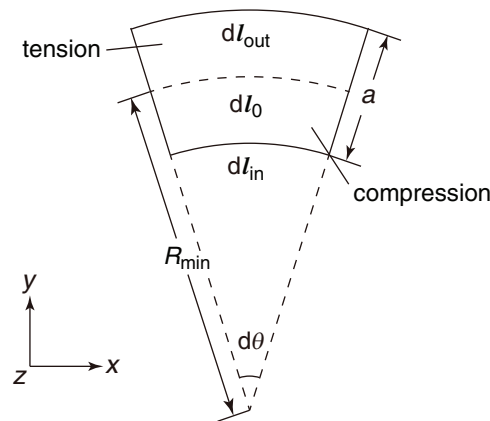


Figure 3: Schematic of the infinitesimal element corresponding to the dash-dotted region in Fig. 2. dl_{out} , dl_0 and dl_{in} denote the length of outer arc, central arc and inner arc, respectively. R_{\min} : curvature radius of the element; $d\theta$: central angle

Assuming that the central arc is free from deformation, we obtain the maximum tensile strain via

$$\epsilon_{\text{tmax}}(L, a) = \frac{dl_{\text{out}}}{dl_0} - 1. \quad (20)$$

$R_{\text{min}}(L)$ decreases with increasing ϵ , and ϵ_{tmax} increases with decreasing $R_{\text{min}}(L)$. When ϵ_{tmax} reaches the intrinsic elastic strain limit of material, ϵ^* , failure occurs, i.e.,

$$\epsilon_{\text{tmax}}(L, a) = \epsilon^*. \quad (21)$$

Eq. (21) together with Eqs. (9) and (17) provides an analytical approach to predict ϵ_f for different beam geometries.

To evaluate the validity of the above nanoscale model and reveal underlying mechanisms, we perform atomistic simulations with a large-scale atomic/molecular massively parallel simulator (LAMMPS) [35]. An accurate embedded-atom method potential is used to describe the atomic interactions in Cu [36]. This potential has been fitted to reproduce physical properties such as stacking fault energy and elastic moduli [36], and widely used in a large number of simulations, including shock compression [37], deformation [38,39], equations of state [40] and cavitation [41,42].

Fig. 1 shows the loading geometry for both buckling and post-buckling simulations. The x -, y - and z -axes are parallel to [110], $[-110]$ and [001], respectively. The left and right ends of the beam are fixed along the y -axis and all of the boundary conditions are non-periodic. In buckling simulations, the beam is first relaxed through energy minimization, and increasing compressive strain is applied along the x -axis at an increment of 0.001. At each strain, a pair of opposite perturbation forces are applied separately along the y -axis to the middle part (green part in Fig. 1a), and energy minimization is conducted after each force is applied. Then ϵ_{cr} is obtained when the beam fails to maintain straight shape. In post-buckling simulations, energy minimization is first conducted after the beam is compressed along the x -axis to 2% and initial geometric imperfection (e.g., ramp displacements, see details in section I of supplementary information, SI-I) is applied to the middle part along the y -axis. The system is then subjected to compressive strain at an increment of 0.001 and the energy of system is minimized after each increment. The temperature in all the simulations is fixed at 0 K. The initial length of beam L_0 is 1000 Å for all the simulations while a varies from 20 to 60 Å.

A set of tensile simulations are carried out to obtain ϵ^* for different a . In these simulations, the beams as in buckling simulations are subjected to tensile strain from 0 with increment of 0.001. ϵ^* is defined as the strain when plastic deformation first occurs. Other simulation conditions are the same as buckling simulations.

3 Results and Discussion

Fig. 4a shows critical strain ϵ_{cr} of buckling simulations for different a , together with predictions of Eq. (3). As expected, simulated ϵ_{cr} increases with increasing a , consistent with Eq. (3). However, the simulation results deviate considerably from classical model. The relative errors of the buckling model relative to the simulation results are shown in Fig. 4b. The relative error decreases with increasing a , ranging from -47% to -17% . The larger errors at small a is due to the larger surface energy per unit volume, since the surface effect is not considered in classical model.

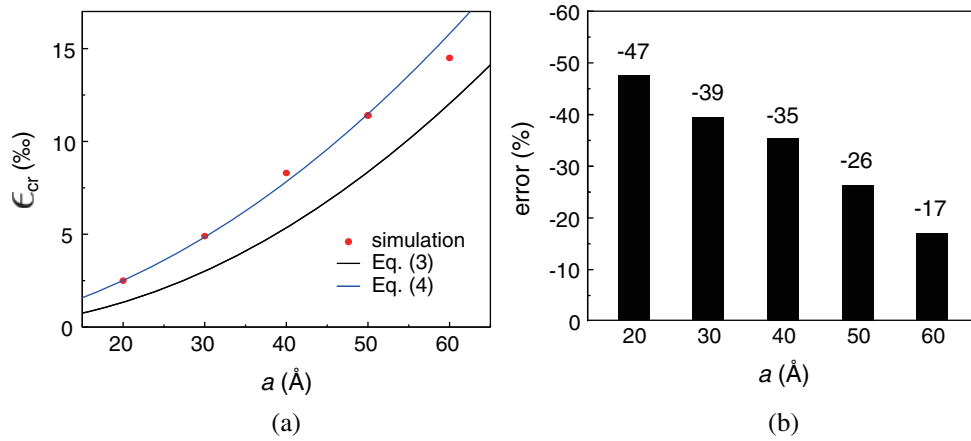


Figure 4: (a) Critical strain ϵ_{cr} for buckling obtained from atomistic simulations, prediction with Eq. (3) and fitting with Eq. (5). (b) Relative errors for predictions with Eq. (3) at different a

The external load translates into surface and structural stresses. Therefore, without considering the surface effect, ϵ_{cr} is underestimated (Fig. 4a). To include the surface effect, the simulation data can be well fitted with Eq. (5) (the blue curve in Fig. 4a, $\tilde{E}^s = 54$ N/m).

For post-buckling, Fig. 5 shows the evolution of average potential energy per atom U_p with applied nominal strain ($a = 40$ Å), together with four representative snapshots. In these atomic configurations, the atom types are characterized with the common neighbor analysis (CNA) method [43,44] and only face-centered cubic (FCC, green) and hexagonal close-packed (HCP, red) atoms are plotted. In the early stage (e.g., $\epsilon < 0.1$), U_p increases with increasing ϵ as a result of the accumulation of elastic energy. The curvature and deflection magnitude of the beam increases and no plastic deformation is found in this stage (1 and 2 in Fig. 5). However, U_p begins to decrease when ϵ exceeds 0.103 and plastic deformation occurs in the corresponding atomic configurations (configuration 3, Fig. 5). The plastic deformation is induced by partial dislocation, and the activated slip systems are $(111)/[\bar{1}\bar{1}2]$ and $(11\bar{1})/[\bar{1}\bar{1}2]$, the same as the ones in Lennard–Jones system under tension [45]. Thus, ϵ_f equals to 0.103 in this simulation. U_p then continues to decrease and the beam begins to crack in following compression process (configuration 4 in Fig. 5).

In our simulations, the maximum deflection w_{max} is obtained as the maximum y coordinate of the beam minus $a/2$. The simulation results of w_{max} are shown in Fig. 6 for different ϵ and a , together with the prediction of Eq. (8). Only data before failure are shown and the arrows indicate the initiation of failure. Failure is not included in the prediction curve. During the initial loading (e.g., $\epsilon < 0.05$), the evolution and equilibrium processes induce differences in geometries for different a . However, as the loading continues to increase, the beam geometries approach the theoretical one and these differences decrease. In our model, w_{max} is determined by L_0 and L (or ϵ , Eq. (8)), and is independent of a . In this sense, the simulations and our model are in good agreement. Nevertheless, w_{max} is less than the model prediction for all the cases we explored by about 2 nm.

Similar to buckling simulations, w_{max} in post-buckling is also influenced by the surface effect [46]. In general, the elastic energy of the nanobeam increases with increasing deflection. If the surface effect is ignored, the work done by the external force F is completely converted into

elastic energy. Considering the surface effects, a shift should be added to the original prediction according to Eq. (13), which is consistent with simulation results (Fig. 6). In our case, the shift constant c equals to 1.7 nm.

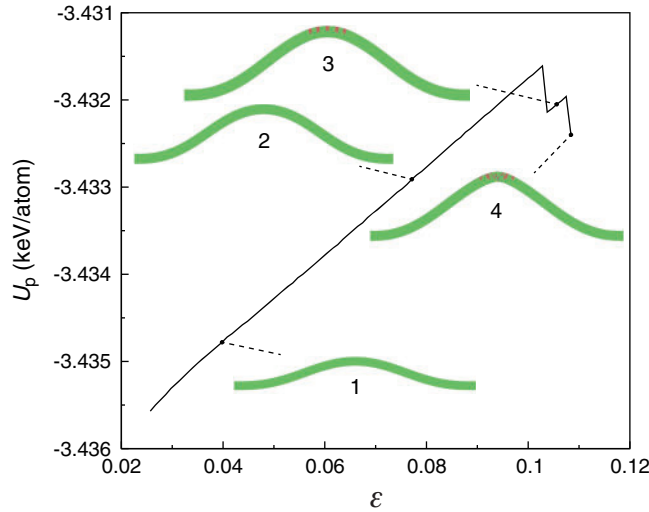


Figure 5: Average potential energy per atom U_p vs. nominal strain ε for post-buckling simulation with $a = 40 \text{ \AA}$. Insets show snapshots at different ε . Green and red atoms represent face-centered cubic (FCC) and hexagonal close-packed (HCP) local packing, respectively

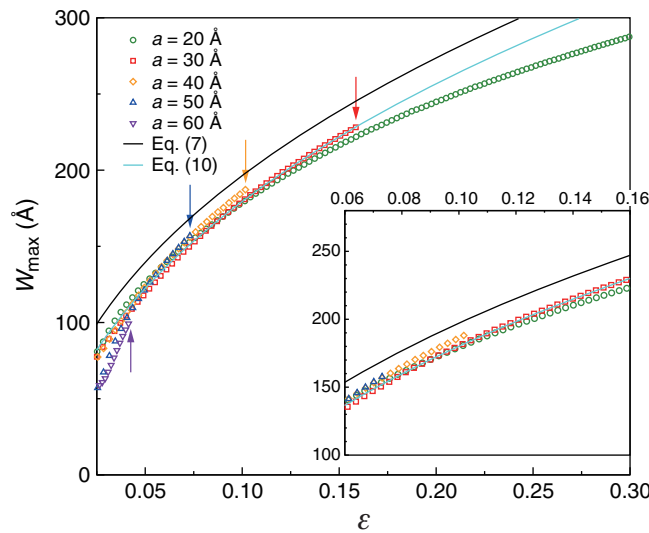


Figure 6: Maximum deflections for different a vs. nominal strain ε obtained from simulations (symbols), predictions of Eq. (8) (black curve) and modification of Eq. (13) (cyan curve). Inset shows an enlarged region of interest. Only data before failure are shown and the arrows indicate the initiation of failure

The nominal failure strain ε_f is also important in practical applications. Here we obtain ε_f from our simulations via the method described above and the results are shown in Fig. 7. Since the beam with $a = 20 \text{ \AA}$ does not show indications of failure during the whole simulation (ε up to 0.3), ε_f is not available in this case. The predictions of our model (Eq. (21)) are also displayed in this figure. The parameter $\epsilon^* = 0.100$ in Eq. (21) is determined by independent tensile simulations. The simulation result is displayed in SI-II. In these tensile simulations, the sample sizes are the same as the nanobeams and the surface would have an effect on the plasticity behavior. Thus the surface effect has already been included in ϵ^* simulations and no additional modification is needed for Eq. (21). As shown in Fig. 7, our model shows good agreement with the simulation results for different a , which indicates our model can accurately predict the failure strain down to 3 nm. Compared with the common solutions (high order buckling curves or assuming a complicated surface system), there are only two parameters (the effective surface Young's modulus \tilde{E}^s and decreased deflection ΔA_s) in this simplified model. The solution based on this model is in good agreement with the results of atomistic simulations (Figs. 6 and 7).

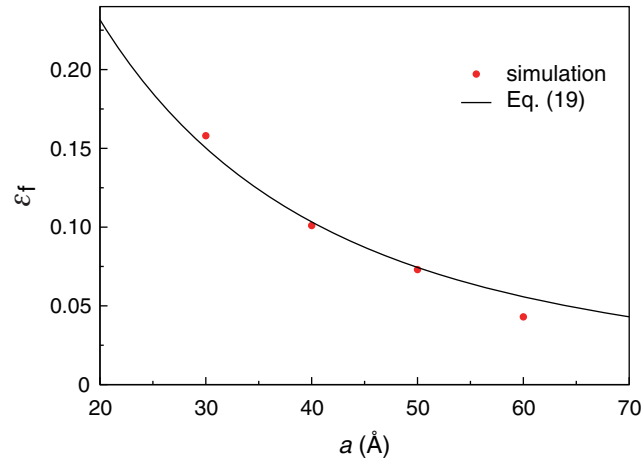


Figure 7: Nominal failure strain ε_f for different a obtained from atomistic simulations and prediction by Eq. (21)

4 Conclusion

A stress-based simplified model is proposed to describe the buckling and post-buckling behaviors of Cu nanobeam under uniaxial compression. The critical strain for buckling, maximum deflection and nominal failure strain for post-buckling are analyzed by this model. We also perform atomistic simulations of the buckling and post-buckling processes. In buckling simulations, the critical strain increases with increasing nanobeam cross section. With the surface effects considered, the simulation results and our model are in good agreement. For post-buckling simulations, the maximum deflection increases with increasing loading strain but stays nearly the same for different cross sections, and the underlying mechanisms are revealed by our model. The maximum deflection is also influenced by surface effects. The nominal failure strains are in good agreement with this simplified model. Our results can be useful for designing related nanodevices in NEMS.

Acknowledgement: The authors wish to express their appreciation to the reviewers for their helpful suggestions which greatly improved the presentation of this paper.

Funding Statement: This work was partially supported by the Scientific Challenge Project of China (Grant No. TZ2018001), and the National Natural Science Foundation of China (Grant No. 11627901).

Conflicts of Interest: The authors declare that they have no conflicts of interest to report regarding the present study.

References

1. Timoshenko, S. P., Gere, J. M. (1985). *Theory of elastic stability*. New York: McGraw-Hill.
2. Budiansky, B. (1974). Theory of buckling and post-buckling behavior of elastic structures. *Advances in Applied Mechanics*, 14, 1–65.
3. Cui, Y., Zhong, Z. H., Wang, D., Wang, W. U., Lieber, C. M. (2003). High performance silicon nanowire field effect transistors. *Nano Letters*, 3(2), 149–152. DOI 10.1021/nl025875l.
4. Xie, R., Montanini, P., Akarvardar, K., Tripathi, N., Haran, B. et al. (2016). A 7 nm finfet technology featuring euv patterning and dual strained high mobility channels. *2016 IEEE International Electron Devices Meeting*, New York, USA. DOI 10.1109/IEDM.2016.7838334.
5. Aydogdu, M. (2009). A general nonlocal beam theory: Its application to nanobeam bending, buckling and vibration. *Physica E*, 41(9), 1651–1655. DOI 10.1016/j.physe.2009.05.014.
6. Eltaher, M. A., Khater, M. E., Emam, S. A. (2016). A review on nonlocal elastic models for bending, buckling, vibrations, and wave propagation of nanoscale beams. *Applied Mathematical Modelling*, 40(5–6), 4109–4128. DOI 10.1016/j.apm.2015.11.026.
7. Liang, X., Hu, S. L., Shen, S. P. (2014). Effects of surface and flexoelectricity on a piezoelectric nanobeam. *Smart Materials and Structures*, 23(3), 035020. DOI 10.1088/0964-1726/23/3/035020.
8. Gheshlaghi, B., Hasheminejad, S. M. (2011). Surface effects on nonlinear free vibration of nanobeams. *Composites Part B: Engineering*, 42(4), 934–937. DOI 10.1016/j.compositesb.2010.12.026.
9. Li, L., Tang, H. S., Hu, Y. J. (2018). The effect of thickness on the mechanics of nanobeams. *International Journal of Engineering Science*, 123, 81–91. DOI 10.1016/j.ijengsci.2017.11.021.
10. Ghayesh, M. H., Farajpour, A. (2019). A review on the mechanics of functionally graded nanoscale and microscale structures. *International Journal of Engineering Science*, 137, 8–36. DOI 10.1016/j.ijengsci.2018.12.001.
11. Hosseini, M., Hadi, A., Malekshahi, A., Shishesaz, M. (2018). A review of size-dependent elasticity for nanostructures. *Journal of Applied and Computational Mechanics*, 49(1), 197–211.
12. Miller, R. E., Shenoy, V. B. (2000). Size-dependent elastic properties of nanosized structural elements. *Nanotechnology*, 11(3), 139–147. DOI 10.1088/0957-4484/11/3/301.
13. Olsson, P. A., Park, H. S. (2011). Atomistic study of the buckling of gold nanowires. *Acta Materialia*, 59(10), 3883–3894. DOI 10.1016/j.actamat.2011.03.012.
14. Jiang, W., Batra, R. (2009). Molecular statics simulations of buckling and yielding of gold nanowires deformed in axial compression. *Acta Materialia*, 57(16), 4921–4932. DOI 10.1016/j.actamat.2009.06.062.
15. Ansari, R., Sahmani, S. (2011). Bending behavior and buckling of nanobeams including surface stress effects corresponding to different beam theories. *International Journal of Engineering Science*, 49(11), 1244–1255. DOI 10.1016/j.ijengsci.2011.01.007.
16. Thai, H. T. (2012). A nonlocal beam theory for bending, buckling, and vibration of nanobeams. *International Journal of Engineering Science*, 52, 56–64. DOI 10.1016/j.ijengsci.2011.11.011.
17. Li, L., Hu, Y. J. (2017). Post-buckling analysis of functionally graded nanobeams incorporating nonlocal stress and microstructure-dependent strain gradient effects. *International Journal of Mechanical Sciences*, 120, 159–170. DOI 10.1016/j.ijmecsci.2016.11.025.

18. Zhang, B., Shen, H. M., Liu, J., Wang, Y. X., Zhang, Y. R. (2019). Deep postbuckling and nonlinear bending behaviors of nanobeams with nonlocal and strain gradient effects. *Applied Mathematics and Mechanics*, 40(4), 515–548. DOI 10.1007/s10483-019-2482-9.
19. Arefi, M., Bidgoli, E. M. R., Dimitri, R., Baccocchi, M., Tornabene, F. (2019). Nonlocal bending analysis of curved nanobeams reinforced by graphene nanoplatelets. *Composites Part B: Engineering*, 166, 1–12. DOI 10.1016/j.compositesb.2018.11.092.
20. Durinck, J., Coupeau, C., Colin, J., Grilhé, J. (2008). Molecular dynamics simulations of buckling-induced plasticity. *Applied Physics Letters*, 93(22), 221904. DOI 10.1063/1.3033552.
21. Ansari, R., Mohammadi, V., Shojaei, M. F., Gholami, R., Sahmani, S. (2014). Postbuckling analysis of timoshenko nanobeams including surface stress effect. *International Journal of Engineering Science*, 75, 1–10. DOI 10.1016/j.ijengsci.2013.10.002.
22. Barati, M. R., Zenkour, A. M. (2019). Thermal post-buckling analysis of closed circuit flexoelectric nanobeams with surface effects and geometrical imperfection. *Mechanics of Advanced Materials and Structures*, 26(17), 1482–1490. DOI 10.1080/15376494.2018.1432821.
23. Ahmed, R. A., Fenjan, R. M., Faleh, N. M. (2019). Analyzing post-buckling behavior of continuously graded fg nanobeams with geometrical imperfections. *Geomechanics and Engineering*, 17(2), 175–180.
24. Gao, Y., Xiao, W. S., Zhu, H. P. (2019). Nonlinear bending and thermal post-buckling behavior of functionally graded piezoelectric nanosize beams using a refined model. *Materials Research Express*, 6(6), 065065. DOI 10.1088/2053-1591/ab0f78.
25. Wu, C. P., Yu, J. J. (2019). A review of mechanical analyses of rectangular nanobeams and single-, double-, and multi-walled carbon nanotubes using eringens' nonlocal elasticity theory. *Archive of Applied Mechanics*, 89(9), 1761–1792.
26. Wang, G. F., Feng, X. Q. (2009). Timoshenko beam model for buckling and vibration of nanowires with surface effects. *Journal of Physics D: Applied Physics*, 42(15), 155411. DOI 10.1088/0022-3727/42/15/155411.
27. Wang, G. F., Feng, X. Q. (2009). Surface effects on buckling of nanowires under uniaxial compression. *Applied Physics Letters*, 94(14), 141913. DOI 10.1063/1.3117505.
28. Ziaee, S. (2015). Small scale effect on linear vibration of buckled size-dependent FG nanobeams. *Ain Shams Engineering Journal*, 6(2), 587–598. DOI 10.1016/j.asej.2014.11.014.
29. Li, Z., Feng, K., Yang, J. S., Tan, L., Lin, H. (2010). Collective buckling of nonuniform nanobeams interacting through an elastic substrate. *Acta Mechanica*, 209(3–4), 285–293. DOI 10.1007/s00707-009-0182-3.
30. Farajpour, A., Ghayesh., M. H., Farokhi, H. (2018). A review on the mechanics of nanostructures. *International Journal of Engineering Science*, 133, 231–263. DOI 10.1016/j.ijengsci.2018.09.006.
31. Zhu, R., Wang, D. Q., Xiang, S. Q., Zhou, Z. Y., Ye, X. Y. (2008). Piezoelectric characterization of a single zinc oxide nanowire using a nanoelectromechanical oscillator. *Nanotechnology*, 19(28), 285712. DOI 10.1088/0957-4484/19/28/285712.
32. Harik, V. (2018). *Mechanics of carbon nanotubes: Fundamentals, modeling and safety*. Cambridge, Massachusetts, US: Academic Press. DOI 10.1016/C2016-0-00799-4.
33. Zhao, Y., Liu, X., Zhu, J., Luo, S. N. (2019). Unusually high flexibility of graphene-Cu nanolayered composites under bending. *Physical Chemistry Chemical Physics*, 21(31), 17393–17399. DOI 10.1039/C9CP02980J.
34. Peng, Z., Chen, S. (2011). Effects of surface roughness and film thickness on the adhesion of a bioinspired nanofilm. *Physical Review E*, 83(5), 051915. DOI 10.1103/PhysRevE.83.051915.
35. Plimpton, S. (1995). Fast parallel algorithms for short-range molecular dynamics. *Journal of Computational Physics*, 117(1), 1–19. DOI 10.1006/jcph.1995.1039.
36. Mishin, Y., Mehl, M. J., Papaconstantopoulos, D. A., Voter, A. F., Kress, J. D. (2001). Structural stability and lattice defects in copper: Ab initio, tight-binding, and embedded-atom calculations. *Physical Review B*, 63(22), 224106. DOI 10.1103/PhysRevB.63.224106.

37. Bringa, E. M., Cazamias, J. U., Erhart, P., Stölken, J., Tanushev, N. et al. (2004). Atomistic shock Hugoniot simulation of single-crystal copper. *Journal of Applied Physics*, *96*(7), 3793–3799. DOI 10.1063/1.1789266.
38. Li, X. Y., Wei, Y. J., Lu, L., Lu, K., Gao, H. J. (2010). Dislocation nucleation governed softening and maximum strength in nano-twinned metals. *Nature*, *464*(7290), 877–880. DOI 10.1038/nature08929.
39. Cahn, J. W., Mishin, Y., Suzuki, A. (2006). Coupling grain boundary motion to shear deformation. *Acta Materialia*, *54*(19), 4953–4975. DOI 10.1016/j.actamat.2006.08.004.
40. Zheng, L. Q., An, Q., Xie, Y., Sun, Z. H., Luo, S. N. (2007). Homogeneous nucleation and growth of melt in copper. *Journal of Chemical Physics*, *127*(16), 164503. DOI 10.1063/1.2790424.
41. Cai, Y., Wu, H. A., Luo, S. N. (2014). Cavitation in a metallic liquid: Homogeneous nucleation and growth of nanovoids. *Journal of Chemical Physics*, *140*(21), 214317. DOI 10.1063/1.4880960.
42. Cai, Y., Huang, J. Y., Wu, H. A., Zhu, M. H., Goddard, W. A. et al. (2016). Tensile strength of liquids: Equivalence of temporal and spatial scales in cavitation. *Journal of Physical Chemistry Letters*, *7*(5), 806–810. DOI 10.1021/acs.jpcllett.5b02798.
43. Tsuzuki, H., Branicio, P. S., Rino, J. P. (2007). Structural characterization of deformed crystals by analysis of common atomic neighborhood. *Computer Physics Communications*, *177*(6), 518–523. DOI 10.1016/j.cpc.2007.05.018.
44. Faken, D., Jónsson, H. (1994). Systematic analysis of local atomic structure combined with 3D computer graphics. *Computational Materials Science*, *2*(2), 279–286. DOI 10.1016/0927-0256(94)90109-0.
45. Cai, Y., Wu, H. A., Luo, S. N. (2018). A loading-dependent model of critical resolved shear stress. *International Journal of Plasticity*, *109*, 1–17. DOI 10.1016/j.ijplas.2018.03.011.
46. Ansari, R., Mohammadi, V., Shojaei, M. F., Gholami, R., Sahmani, S. (2013). Postbuckling characteristics of nanobeams based on the surface elasticity theory. *Composites Part B: Engineering*, *55*, 240–246. DOI 10.1016/j.compositesb.2013.05.040.